From relativistic quantum fields to condensed matter and back again: updating the Gross–Neveu phase diagram

2006 J. Phys. A: Math. Gen. 39 12707

(http://iopscience.iop.org/0305-4470/39/41/S04)

INSTITUTE OF PHYSICS PUBLISHING JOURNAL OF PHYSICS A: MATHEMATICAL AND GENERAL

J. Phys. A: Math. Gen. **39** (2006) 12707–12734 doi:10.1088/0305-4470/39/41/S04

From relativistic quantum fields to condensed matter and back again: updating the Gross–Neveu phase diagram

Michael Thies

Institut für Theoretische Physik III, Universität Erlangen-Nürnberg, Staudtstr. 7, 91058 Erlangen, Germany

E-mail: thies@theorie3.physik.uni-erlangen.de

Received 8 March 2006
Published 27 September 2006
Online at stacks.iop.org/JPhysA/39/12707

Abstract

During the last few years, the phase diagram of the large N Gross–Neveu model in $1+1$ dimensions at finite temperature and chemical potential has undergone a major revision. Here, we present a streamlined account of this development, collecting the most important results. Quasi-one-dimensional condensed matter systems like conducting polymers provide real physical systems which can be approximately described by the Gross–Neveu model and have played some role in establishing its phase structure. The kink–antikink phase found at low temperatures is closely related to inhomogeneous superconductors in the Larkin–Ovchinnikov–Fulde–Ferrell phase. With the complete phase diagram at hand, the Gross–Neveu model can now serve as a firm testing ground for new algorithms and theoretical ideas.

PACS numbers: 03.70.+k, 11.10.−z

1. Introduction

In its original form, the Gross–Neveu (GN) model [1] is a relativistic, renormalizable quantum field theory (QFT) of N species of self-interacting fermions in $1+1$ dimensions with Lagrangian

$$\mathcal{L} = \sum_{n=1}^{N} \bar{\psi}^{(n)}(\mathrm{i}\gamma^{\mu}\partial_{\mu} - m_0)\psi^{(n)} + \frac{1}{2}g^2\left(\sum_{n=1}^{N}\bar{\psi}^{(n)}\psi^{(n)}\right)^2 . \tag{1}$$

The bare mass term $\sim m_0$ explicitly breaks the discrete chiral symmetry $\psi \to \gamma^5\psi$ of the massless model. The interaction term can be generalized to acquire a continuous chiral symmetry as in the Nambu–Jona–Lasinio (NJL) model, but we shall not consider this option here. As far as the phase diagram is concerned, the 't Hooft limit $N \to \infty$, $g^2 \sim 1/N$ is most instructive. The reason is the following. In $1+1$ dimensions, classic no-go theorems

forbid spontaneous breaking of a continuous symmetry at zero temperature or of a discrete symmetry at finite temperature [2, 3]. Although mean-field theory often predicts these effects, fluctuations are expected to destroy any long range order. Provided that one defines the model by letting $N \to \infty$ before taking the thermodynamic limit, these fluctuations are suppressed and a richer phase structure becomes accessible [4]. We follow this line of reasoning here.

Like in a previous pedagogical review article [5] which the present paper is meant to update, we work canonically, couching the theory in the language of the relativistic Hartree–Fock (HF) approximation. It is formally equivalent to the semi-classical functional integral approach but conceptually simpler. Physically, it emphasizes the fact that the Dirac sea is an interacting many-fermion system [6, 7], thereby making it somewhat easier to switch back and forth between the relativistic QFT and condensed matter physics literature.

Let us now briefly recall the motivation for studying the Lagrangian (1). QFT models for which one can construct the exact renormalized phase diagram are extremely scarce and worth investigating on theoretical grounds, even if they are far from being realistic. As a matter of fact, in spite of its simple Lagrangian, the GN model shares many non-trivial properties with quantum chromodynamics (QCD), notably asymptotic freedom, dimensional transmutation, meson and baryon bound states, chiral symmetry breaking in the vacuum as well as its restoration at high temperature and density. Perhaps even more surprising and less widely appreciated is the fact that GN-type models have enjoyed considerable success in describing a variety of quasi-one-dimensional condensed matter systems such as the Peierls–Fröhlich model, conducting polymers like polyacetylene or inhomogeneous superconductors.

The title of this paper has the following background: originally, the kink and kink–antikink baryons first derived in QFT by Dashen, Hasslacher and Neveu [8] have been useful for understanding the role of solitons and polarons in electrical conductivity properties of doped polymers [9]. In the following years, a lot of progress was made in condensed matter theory towards understanding polaron crystal structures. This in turn helped us to construct the full phase diagram of the relativistic QFT. However, in order not to confuse the issues, we shall first discuss the GN model without reference to condensed matter physics and comment on the relationship only towards the end.

Our last remark about the motivation concerns the restriction to 1 + 1 dimensions. At first glance, this looks very unrealistic. However, most of the work discussed below has to do with finite chemical potential. In the presence of a Fermi surface, a kind of dimensional reduction takes place which has been exploited for instance in high-density effective theory (HDET) to QCD (see [10] for a review). It also manifests itself through the well-known fact that Cooper pairing in superconductivity occurs for arbitrarily weak attraction, just like in one space dimension. Hence, from the physics point of view, the restriction to 1 + 1 dimensions is perhaps a better idea in the presence of fermionic matter than naively thought.

The Lagrangian (1) has two bare parameters, g^2 and m_0. In the process of regularization and renormalization, all observables can be expressed in terms of two physical parameters m and γ. The relation to the bare quantities and the ultra-violet (UV) cut-off Λ is given by the vacuum gap equation

$$\frac{\pi}{Ng^2} = \gamma + \ln\frac{\Lambda}{m}, \qquad \gamma := \frac{\pi}{Ng^2}\frac{m_0}{m}. \tag{2}$$

Whereas the physical fermion mass m in the vacuum merely provides the overall mass scale and can be set equal to 1, the second parameter γ (called 'confinement parameter' in condensed matter physics) parametrizes different physical theories. It measures the amount of explicit chiral symmetry breaking and vanishes in the massless ($m_0 = 0$) limit. Note that it can also

be expressed in terms of the physical fermion masses at bare mass m_0 and in the chiral limit,

$$\gamma = \ln\left(\frac{m[m_0]}{m[0]}\right). \tag{3}$$

The main subject of this paper is the full phase diagram of the massive GN model as a function of temperature T, chemical potential μ and confinement parameter γ. The original works date from 1985 for the massless [11] and 1995 for the massive case [12] (see also [13] for earlier, partial results). As has become clear by now, the assumption that the scalar condensate $\langle\bar{\psi}\psi\rangle$ is spatially homogeneous made in these works is too restrictive. It misses important physics closely related to the existence of kink–antikink baryons in the GN model. In the present paper, we describe how this problem has been cured. This is not a small correction, but requires a substantial new effort. A homogeneous condensate acts like a mass and reduces the thermodynamics essentially to that of a massive, free relativistic Fermi gas, the mass being determined self-consistently. By contrast, solving the Dirac equation with a periodic potential and establishing self-consistency is a highly non-trivial task, even in $1+1$ dimensions. Due to a number of lucky circumstances, this is nevertheless possible in the case at hand, to a large extent even analytically.

In our recent papers, we had to proceed from special cases to more general ones (treating $m_0 = 0$ before $m_0 \neq 0, T = 0$ before $T \neq 0$) in order to reduce the problem to manageable size. Now that the original technical difficulties have been overcome, we invert this chronological order. We start from the most general case, i.e., the massive GN model at finite temperature and chemical potential, and specialize further wherever additional analytical results or physics insights are available. In this way, we can hopefully convey a more coherent picture of what has been learned in the meantime.

This paper is organized as follows. In section 2, we remind the reader of the state of the art around the year 2000 and recall our criticism on the widely accepted phase diagram of the GN model at that time. We motivate the analytical form of the correct self-consistent HF potential in section 3 and sketch the calculation of the grand canonical potential and the proof of self-consistency in section 4. Section 5 exhibits the revised phase diagram 'in full glory'. In the following four sections, we have added various results in the form of figures and analytical formulae which have been obtained in simpler special cases, letting one or both of the parameters T and γ go to zero. If we take the low-density limit $\rho \to 0$ at zero temperature, we also recover the properties of individual baryons as summarized in section 10. Section 11 contains a brief overview of the many cross-relations between the GN model as a relativistic QFT and the theory of certain quasi-one-dimensional condensed matter systems. It is followed by our concluding remarks in section 12.

2. Reminder of the situation five years ago

Let us briefly recall the phase diagram of the GN model as it had been widely accepted by the year 2000. This is necessary to put the recent development into perspective. Besides, we will see that the results remain valid in some regions of the phase diagram, including some critical curves. The most basic quantity at finite temperature T and chemical potential μ is the grand canonical potential. In the large N limit, it can be computed either canonically via the relativistic HF approach or by using semi-classical functional integral methods. In the more popular path integral approach, one introduces an auxiliary bosonic field σ and integrates out the fermions exactly (Gaussian integral over Grassmann variables), then applies a saddle point approximation to the remaining bosonic functional integral. In the original analysis at $\gamma = 0$ [11] and its generalization to finite bare fermion masses [12], it has been assumed

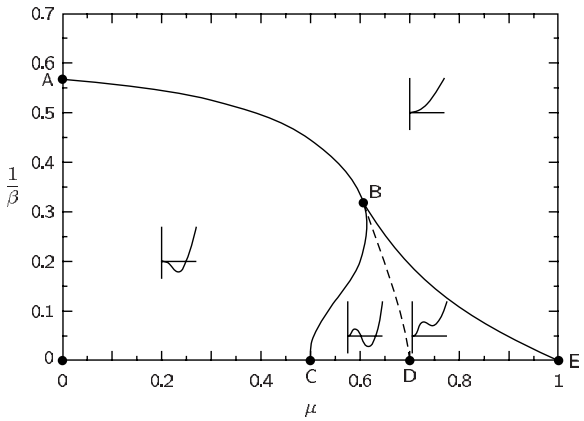

Figure 1. 'Old' phase diagram of the massless GN model, assuming unbroken translational symmetry. For a discussion, see the main text. Units of m; adapted from [11].

that the classical value of σ (i.e., the saddle point) is spatially constant, yielding a (μ, T)-dependent dynamical fermion mass M. This mass is found by minimizing the renormalized grand canonical potential density

$$\Psi = \frac{M^2}{2\pi}\left(\ln M - \frac{1}{2}\right) + \gamma\left(\frac{M^2}{2\pi} - \frac{M}{\pi}\right) - \frac{1}{\beta\pi}\int_0^\infty \mathrm{d}q\, \ln[(1+\mathrm{e}^{-\beta(E-\mu)})(1+\mathrm{e}^{-\beta(E+\mu)})] \tag{4}$$

$(\beta = 1/T, m = 1, E = \sqrt{q^2+M^2})$ with respect to M. Equivalently, one can solve the self-consistency condition for the (thermal) fermion condensate,

$$M = m_0 - Ng^2\langle\bar\psi\psi\rangle_{\mathrm{th}}. \tag{5}$$

Depending on the parameters (γ, μ, T), Ψ possesses one or two local minima with the possibility of a first-order phase transition. The phase diagram in the chiral limit $\gamma = 0$ is shown in figure 1, whereas the 3D plot in figure 2 exhibits the phase structure in the full (γ, μ, T)-space. Let us first look at figure 1. The line AB is a critical line of second-order transitions (the thermodynamic potential changes from one minimum to a maximum and a minimum). The point B is a tricritical point located at $1/\beta = 0.3183$, $\mu = 0.6082$ (all numbers here are in units of m); it separates the second-order line from a first-order line BD along which the potential has two degenerate minima and a maximum. The endpoint D lies at $\mu = 1/\sqrt{2}$ where the $T = 0$ phase transition occurs. Lines BC and BE are boundaries of metastability; when crossed, the potential acquires or loses a second minimum. In region OABD, chiral symmetry is broken and the fermions are massive; the outside region has unbroken chiral symmetry and massless fermions. As the parameter γ is switched on, the second-order line AB disappears in favour of a cross-over where the fermion mass changes rapidly, but smoothly. The first-order line on the other hand survives, ending at a critical point. If plotted against γ, these critical points lie on the third curve $\mathrm{P_tC}$ emanating from the tricritical point as shown in figure 2. For $\gamma > 0$, the effective fermion mass M is everywhere different from zero. If one crosses the shaded critical 'sheet' in figure 2, the mass changes discontinuously, dropping with increasing chemical potential.

These results looked rather convincing and indeed have been confirmed repeatedly by other authors, see e.g. [15, 16]. Nevertheless, they suffer from one disease which was pointed out in [5]. The GN model possesses baryons (multi-fermion bound states) due to binding

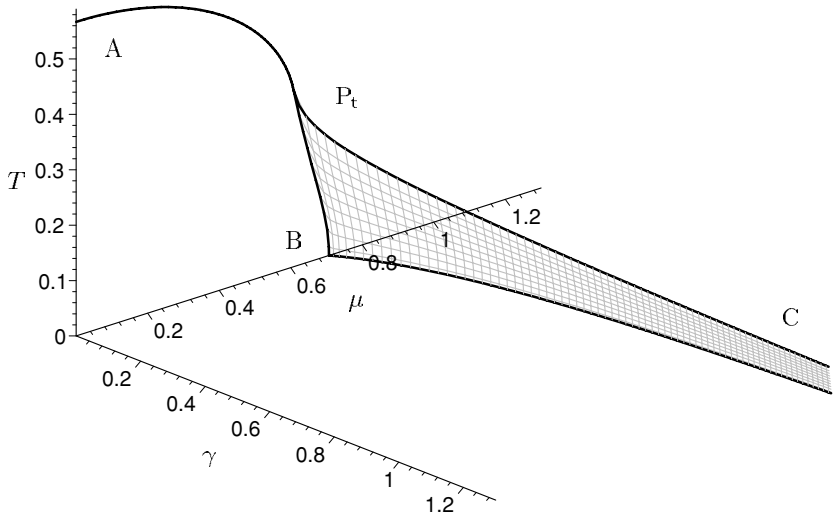

Figure 2. 'Old' phase diagram of the massive GN model as a function of γ, μ, T, assuming unbroken translational symmetry [12, 14, 30]. The various phase boundaries are explained in the main text. The $\gamma = 0$ plane corresponds to figure 1, the tricritical point P_t to the point B there.

effects which are not $1/N$ suppressed. Consider the low-density limit of baryonic matter at $T = 0$. Since the baryon–baryon interaction is known to be short ranged and repulsive, one expects widely spaced baryons in the low-density limit, implying the following slope of the energy density at the origin:

$$\left.\frac{\partial \mathcal{E}}{\partial \rho}\right|_{\rho=0} = M_B. \tag{6}$$

Here, M_B is the baryon mass. Conversely, since equation (6) is just the chemical potential at $T = 0$, the phase transition at $T = 0$ should occur at the critical chemical potential $\mu = M_B$. The phase diagrams in figures 1 and 2 are in conflict with this expectation. At $\gamma = 0$, for instance, the first-order phase transition takes place at $\mu = 1/\sqrt{2}$, whereas the baryon mass is $M_B = 2/\pi$ (always taking out a trivial factor of N). At the time of writing the article [5], it was already clear that the problem had to do with the assumption of translational invariance. Indeed, if the single baryon breaks translational invariance, there is no good reason why this symmetry should not be broken at finite baryon densities as well. (One can actually understand the value of $1/\sqrt{2}$ of the critical chemical potential in terms of a droplet model for baryons, characteristic for the mixed phase at low density. The argument which was first developed in the context of the GN model with continuous chiral symmetry [17] applies here as well.)

Incidentally, a related observation had already been made in 1987 by Karsch *et al* whose numerical lattice calculation gave first hints that kink–antikink configurations play a role in the phase diagram at low density [18]. However, the authors concluded erroneously that there was a problem with the mean-field approach, an opinion which has often been voiced in the literature since then. This calculation was too crude to determine the phase diagram quantitatively, in particular the statements about the order of the phase transitions are no longer tenable, as we now know.

Unfortunately, it is not easy to relax the assumption of a constant potential, since this requires a major new effort. This can already be judged from the rather involved single baryon problem [8] which must be contained as a limit in the full calculation. Which potential $S(x)$

should replace the constant mass M so as to cure the aforementioned discrepancy? This will be answered in the next section.

3. How to choose the right ansatz for the scalar potential

Our strategy within the relativistic HF approach is extremely simple in principle: guess the functional form of the HF potential and verify its self-consistency. At finite density, we expect the appearance of a regular array of baryons, hence we will be searching for periodic solutions. But what guidance do we have to pick the right ansatz? Is there any reason at all to assume that the exact potential can be given in closed analytical form? The following heuristic considerations should be of some help.

Owing to the $(\bar\psi\psi)^2$-interaction in the Lagrangian (1), the Dirac–HF equation for the GN model assumes the form

$$\left(-\mathrm{i}\gamma^5\frac{\partial}{\partial x}+\gamma^0 S(x)\right)\psi(x)=E\psi(x) \tag{7}$$

with real scalar potential $S(x)$. The representation

$$\gamma^0=-\sigma_1,\qquad \gamma^1=\mathrm{i}\sigma_3,\qquad \gamma^5=\gamma^0\gamma^1=-\sigma_2 \tag{8}$$

of the γ-matrices has the advantage that the equations for the upper and lower components $\phi_\pm$ of the Dirac spinor ψ can be decoupled by simply applying the Dirac Hamiltonian twice,

$$\left(-\frac{\partial^2}{\partial x^2}\mp\frac{\partial}{\partial x}S+S^2\right)\phi_\pm=E^2\phi_\pm. \tag{9}$$

Equation (9) states that the Schrödinger-type Hamiltonians with potentials $U_\pm=S^2\pm S'$ have the same spectra, a textbook example of supersymmetric quantum mechanics with superpotential S. $S(x)$ in turn depends on the eigenfunctions ψ_α and eigenvalues E_α through a self-consistency relation

$$-\frac{1}{Ng^2}(S(x)-m_0)=\langle\bar\psi\psi\rangle_{\mathrm{th}}=\sum_\alpha\bar\psi_\alpha(x)\psi_\alpha(x)\frac{1}{\mathrm{e}^{\beta(E_\alpha-\mu)}+1}. \tag{10}$$

It generalizes equation (5) to an x-dependent scalar potential.

Let us first recall the results for single baryons in the massive GN model [19, 20]. The scalar potential for a baryon has the form

$$S(x)=1+y[\tanh(yx-c_0)-\tanh(yx+c_0)],\qquad c_0=\tfrac{1}{2}\mathrm{artanh}\,y. \tag{11}$$

The parameter y depends on the bare fermion mass and the number of valence fermions. Here, the corresponding isospectral potentials $U_\pm$ in the second-order equation (9) are given by the simplest Pöschl–Teller potential [21]

$$S^2\pm S'=-\frac{2y^2}{\cosh^2(yx\pm c_0)} \tag{12}$$

and differ only by a translation in space. The distinguishing feature of potential (12) is the fact that it is reflectionless; indeed, this is the unique reflectionless potential with a single bound state. It is well known that static solutions of the GN model must correspond to reflectionless Schrödinger potentials [8, 22]. The fact that the ansatz (11) leads to self-consistency is therefore quite plausible.

Take now a lattice of infinitely many, equidistant Pöschl–Teller potential wells. As pointed out in [23, 24], the lattice sum can be performed yielding a Lamé-type potential,

$$\sum_{n=-\infty}^{\infty}\frac{1}{\cosh^2(x-nd)}=\left(\frac{2\kappa\mathbf{K}'}{\pi}\right)^2\left\{\frac{\mathbf{E}'}{\kappa^2\mathbf{K}'}-\mathrm{sn}^2\left(\frac{2\mathbf{K}'}{\pi}x\right)\right\}. \tag{13}$$

($\mathbf{K}$, $\mathbf{E}$ denote complete elliptic integrals of first and second kinds, $\mathbf{K}'$, $\mathbf{E}'$ the complementary ones with argument $\kappa' = \sqrt{1-\kappa^2}$, sn a Jacobi elliptic function of modulus κ). Comparing the spatial period of both sides of equation (13), we can relate d and κ via

$$d = \pi \frac{\mathbf{K}}{\mathbf{K}'}. \tag{14}$$

How does the fact that the single potential wells (12) are reflectionless manifest itself in the periodic extension (13)? This has been answered long time ago [25, 26]: the periodic potential has a single gap (or, in general, a finite number of gaps), in contrast to generic periodic potentials with infinitely many gaps. Thus, reflectionless potentials generalize to 'finite band potentials' as one proceeds from a single well to a periodic array. In the same way as the sech^2-potential is the unique reflectionless potential with one bound state, the sn^2-potential is the unique single band potential. Guided by these considerations, let us try to find the most general superpotential of the (single gap) Lamé potential. After a scale transformation

$$S(x) = A\tilde{S}(\xi), \qquad \xi = Ax, \tag{15}$$

$U_\pm(x) = A^2\tilde{U}_\pm(\xi)$ should assume the form of the Lamé potential plus constant, up to a possible shift of the rescaled coordinate ($\xi_+ = \xi + b$),

$$\tilde{U}_+ = \tilde{S}^2 + \tilde{S}' = 2\kappa^2 \mathrm{sn}^2\xi_+ + \eta, \qquad \tilde{U}_- = \tilde{S}^2 - \tilde{S}' = 2\kappa^2 \mathrm{sn}^2\xi + \eta, \tag{16}$$

or, equivalently,

$$\tilde{S}^2 = \kappa^2(\mathrm{sn}^2\xi_+ + \mathrm{sn}^2\xi) + \eta, \qquad \tilde{S}' = \kappa^2(\mathrm{sn}^2\xi_+ - \mathrm{sn}^2\xi). \tag{17}$$

Let us try to solve equations (17) for $\tilde{S}$ and η. We differentiate the first equation (17) using

$$(\mathrm{sn}\,\xi)' = \mathrm{cn}\,\xi\,\mathrm{dn}\,\xi \tag{18}$$

and divide the result by the second equation, obtaining

$$\tilde{S}(\xi) = \frac{\mathrm{sn}\,\xi_+\mathrm{cn}\,\xi_+\mathrm{dn}\,\xi_+ + \mathrm{sn}\,\xi\,\mathrm{cn}\,\xi\,\mathrm{dn}\,\xi}{\mathrm{sn}^2\,\xi_+ - \mathrm{sn}^2\,\xi}. \tag{19}$$

By specializing equation (17) to $\xi = 0$, we can also determine the constant η

$$\eta = \frac{1}{\mathrm{sn}^2 b} - 1 - \kappa^2. \tag{20}$$

Incidentally, $\tilde{S}$ can be cast into the somewhat simpler form

$$\tilde{S}(\xi) = \kappa^2 \mathrm{sn}\,b\,\mathrm{sn}\,\xi\,\mathrm{sn}\,(\xi + b) + \frac{\mathrm{cn}\,b\,\mathrm{dn}\,b}{\mathrm{sn}\,b}. \tag{21}$$

The scale factor A in equation (15) is not constrained by these considerations, so that the final answer for $S(x)$ depends on three real parameters A, κ, b. Thus, we conclude that the potential (15, 19) is the most general Dirac potential leading to a single gap Lamé potential (plus constant) in the corresponding second-order equations. This explains why it is a good starting point for finding periodic, static solutions, and has turned out to be the key to the phase diagram of the massive GN model. Incidentally, we did not derive the ansatz for $S(x)$ in this way originally, but took it over from a mathematically closely related problem which had already been solved in condensed matter physics, the bipolaron crystal in non-degenerate conducting polymers. We will have more to say about this relationship in section 11. Also note that the simple and intuitive relation between the single baryon and the crystal exhibited in equation (13) is deeply hidden in the corresponding Dirac potentials (11) and (15), (19) due to the nonlinear, non-local relationship between S and $U_\pm$.

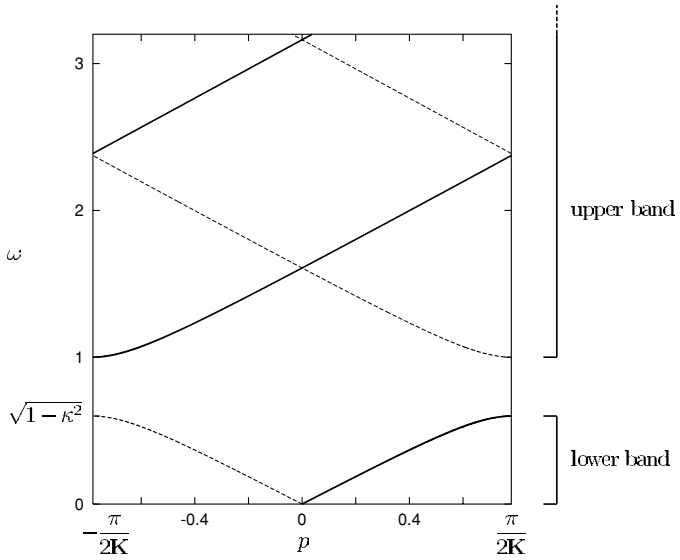

Figure 3. The dispersion relation of the Lamé potential for $\kappa = 0.8$, showing a single gap; $\omega = E/A$ and $p = q/A$ are (reduced) energy and Bloch momentum, respectively (from [28]).

Inserting our ansatz into equation (9), we arrive by construction at the single gap Lamé equation in the form

$$\left(-\frac{\partial^2}{\partial\xi^2} + 2\kappa^2 \mathrm{sn}^2(\xi + (b \mp b)/2)\right)\phi_\pm = \mathcal{E}\phi_\pm. \tag{22}$$

Using equation (20), the relation between Dirac eigenvalues E and Lamé eigenvalues $\mathcal{E}$ is

$$\mathcal{E} = \frac{E^2}{A^2} - \frac{1}{\mathrm{sn}^2 b} + 1 + \kappa^2. \tag{23}$$

The solutions of equation (22) are well known since [27]. The eigenfunctions are fairly complicated, although they can still be given in closed form,

$$\phi_+(\xi) = \mathcal{N}\frac{\mathrm{H}(\xi+\alpha)}{\Theta(\xi)}\,\mathrm{e}^{-\mathrm{Z}(\alpha)\xi}. \tag{24}$$

Here, H, Θ and Z are the Jacobi eta, theta and zeta function, respectively. The parameter α is related to the energy and Bloch momentum. An example of the dispersion relation is shown in figure 3.

The fact that $S(x)$ is a finite band potential is important for getting self-consistency. At the same time, it makes the problem analytically tractable. Of course, at this point one cannot be sure that the simplest finite band potential is sufficient to solve the massive GN model at all temperatures and chemical potential, but this is what eventually will come out.

4. Minimizing the grand potential and self-consistency condition

Having picked the ansatz for the scalar potential $S(x)$, we now have to minimize the grand potential with respect to the three parameters A, κ, b and verify that it implies self-consistency of the $\bar\psi\psi$-condensate. In HF approximation, the grand canonical potential density per flavour

consists of the independent particle contribution Ψ_1 and the double-counting correction to the interaction Ψ_2,

$$\Psi = \Psi_1 + \Psi_2, \qquad \Psi_1 = -\frac{1}{\beta\pi}\int_0^{\Lambda/2} \mathrm{d}q\, \ln[(1+\mathrm{e}^{-\beta(E-\mu)})(1+\mathrm{e}^{\beta(E+\mu)})],$$
$$\Psi_2 = \frac{1}{2Ng^2\ell}\int_0^{\ell} \mathrm{d}x (S(x)-m_0)^2, \qquad \ell = 2\mathbf{K}/A \tag{25}$$

(in the path integral approach, Ψ_1 and Ψ_2 correspond to the fermion determinant and the tree level term, respectively). $\Lambda/2$ is an UV cut-off which will eventually be sent to infinity, ℓ is the spatial period of $S(x)$, E is the single particle energy.

In Ψ_2, we need the spatial averages of S and S^2. It is convenient to introduce three basic functions of b and κ,

$$s = \frac{1}{\mathrm{sn}^2 b}, \qquad t = \frac{\mathrm{cn}\, b\, \mathrm{dn}\, b}{\mathrm{sn}^3 b}, \qquad u = 1 - \frac{\mathbf{E}}{\mathbf{K}}, \tag{26}$$

where s and t are related by

$$t^2 = s(s-1)(s-\kappa^2). \tag{27}$$

The spatial averages can then be written in the compact form

$$\langle S\rangle = A(\mathrm{Z} + t/s), \qquad \langle S^2\rangle = A^2(s - 1 + 2u - \kappa^2) \tag{28}$$

with Jacobi's zeta function $\mathrm{Z} = \mathrm{Z}(b,\kappa)$.

Turning to Ψ_1, let us first transform the momentum integral into an integral over Dirac energies. The density of states for the Lamé potential [29] implies a change of integration measure ($p = q/A$, $\omega = E/A$)

$$\frac{\mathrm{d}p}{\mathrm{d}\omega} = \frac{\omega(\omega^2 - s + u)}{\pm\sqrt{W}}, \qquad W = (\omega^2 - s + 1)(\omega^2 - s + \kappa^2)(\omega^2 - s), \tag{29}$$

where the plus sign refers to the upper band, the minus sign to the lower band. With the shorthand notation

$$a = \beta A, \qquad \nu = \mu\beta, \tag{30}$$

Ψ_1 can be written as the following integral over the allowed bands:

$$\pi\beta^2\Psi_1 = -a\left(\int_{\sqrt{s-1}}^{\sqrt{s-\kappa^2}} \mathrm{d}\omega + \int_{\sqrt{s}}^{\Lambda_\omega} \mathrm{d}\omega\right)\frac{\mathrm{d}p}{\mathrm{d}\omega}\ln[(1+\mathrm{e}^{-a\omega+\nu})(1+\mathrm{e}^{a\omega+\nu})]. \tag{31}$$

The energy cut-off Λ_ω has to be computed from the momentum cut-off $\Lambda/2$ and equation (29),

$$\Lambda_\omega = \frac{\Lambda}{2A} + \frac{A\langle\tilde{S}^2\rangle}{\Lambda} + O(\Lambda^{-3}). \tag{32}$$

Due to the quadratic divergence of the integral, it is necessary to keep the next-to-leading order term here. Following references [28, 30], we combine the integral over both energy bands as well as over positive and negative energy modes into the real part of a line integral in the complex ω-plane. The path of integration runs infinitesimally above or below the real axis,

$$\pi\beta^2\Psi_1 = -a\lim_{\epsilon\to 0}\mathrm{Re}\int_{-\Lambda_\omega+\mathrm{i}\epsilon}^{\infty+\mathrm{i}\epsilon}\mathrm{d}\omega\frac{\omega(\omega^2-s+u)}{\sqrt{W}}\ln(1+\mathrm{e}^{-a\omega+\nu}). \tag{33}$$

We have to minimize Ψ with respect to A, b, κ for fixed μ, β, γ, a rather tedious task at first glance. In order to simplify the computations, we use the freedom to minimize Ψ with respect to any other set of independent variables. Specifically, we propose to replace A, b, κ by the

spatial averages $\langle S\rangle$, $\langle S^2\rangle$ and the spatial period ℓ of S, see equations (25) and (28). It turns out that these variables are extremely convenient for the proof of self-consistency. The stationarity conditions for the grand potential then read

$$\frac{\partial}{\partial\langle S\rangle}\pi\beta^2\Psi = \beta F_0 = 0, \qquad \frac{\partial}{\partial\langle S^2\rangle}\pi\beta^2\Psi = \beta^2 F_1/2 = 0, \qquad \frac{\partial}{\partial\ell}\pi\beta^2\Psi = a^2 F_2/\ell = 0, \tag{34}$$

where we have introduced functions F_i which play a key role in our approach. The derivatives with respect to the new, composite variables can be taken trivially in the case of Ψ_2 since

$$\Psi_2 = \frac{1}{2Ng^2}\big(\langle S^2\rangle - 2m_0\langle S\rangle + m_0^2\big). \tag{35}$$

Unfortunately, this is not true for Ψ_1 available only in terms of the original variables A, b, κ in equation (33). In order to compute F_i, we therefore invoke the chain rule,

$$\begin{pmatrix}\partial_b\\ \partial_A\\ \partial_\kappa\end{pmatrix}\pi\beta^2\Psi = \begin{pmatrix}\partial_b\langle S\rangle & \partial_b\langle S^2\rangle & \partial_b\ell\\ \partial_A\langle S\rangle & \partial_A\langle S^2\rangle & \partial_A\ell\\ \partial_\kappa\langle S\rangle & \partial_\kappa\langle S^2\rangle & \partial_\kappa\ell\end{pmatrix}\begin{pmatrix}\beta F_0\\ \beta^2F_1/2\\ a^2F_2/\ell\end{pmatrix}. \tag{36}$$

Upon evaluating and inverting the Jacobian matrix on the right-hand side of equation (36), F_i can be expressed in terms of directly computable derivatives of Ψ. After some algebra [30], we arrive at

$$\begin{aligned}
F_0 &= -\frac{\pi\beta m_0}{Ng^2} - t\mathrm{Re}\lim_{\varepsilon\to0^+}\int_{-\infty+\mathrm{i}\varepsilon}^{\infty+\mathrm{i}\varepsilon}\mathrm{d}\omega\left(\frac{\partial}{\partial\omega}\frac{1}{\sqrt{W}}\right)\ln(1+\mathrm{e}^{-a\omega+\nu}),\\
F_1 &= \frac{\pi}{Ng^2} - 1 + \frac{1}{a}\mathrm{Re}\lim_{\varepsilon\to0^+}\int_{-\frac{\Lambda\beta}{2a}+\mathrm{i}\varepsilon}^{\infty+\mathrm{i}\varepsilon}\mathrm{d}\omega\left(\frac{\partial}{\partial\omega}\frac{\omega^2}{\sqrt{W}}\right)\ln(1+\mathrm{e}^{-a\omega+\nu}),\\
F_2 &= \frac{1}{a}\mathrm{Re}\lim_{\varepsilon\to0^+}\int_{-\infty+\mathrm{i}\varepsilon}^{\infty+\mathrm{i}\varepsilon}\mathrm{d}\omega\left[\frac{\omega(\omega^2-s+u)}{\sqrt{W}}\right.\\
&\qquad\left. -\frac{\partial}{\partial\omega}\frac{tZ-u\omega^2+(\omega^2-s+1)(\omega^2-s+\kappa^2)}{\sqrt{W}}\right]\ln(1+\mathrm{e}^{-a\omega+\nu}).
\end{aligned} \tag{37}$$

All three functions F_i vanish at the minimum of the thermodynamic potential (25).

Equations (33), (35) and (37) are the basis for our computations. They are not yet in a form suitable for numerical calculations since they still involve bare parameters and a cut-off, but the present form is illuminating with respect to self-consistency. We therefore first turn to the issue of self-consistency.

The self-consistency condition for the scalar potential $S(x)$ was given in equation (10). For a single mode, $\bar\psi\psi$ reads [31]

$$\bar\psi\psi = \frac{\omega\tilde S - t/\omega}{\omega^2 - s + u}. \tag{38}$$

We transform the thermal expectation value of $\bar\psi\psi$ once again into a complex integral,

$$\begin{aligned}
\langle\bar\psi\psi\rangle_{\mathrm{th}} &= \frac{1}{\pi}\int_0^{\Lambda/2}\mathrm{d}q\;\bar\psi\psi\left(\frac{1}{\mathrm{e}^{\beta(E-\mu)}+1} - \frac{1}{\mathrm{e}^{-\beta(E+\mu)}+1}\right)\\
&= \frac{A}{\pi}\mathrm{Re}\lim_{\varepsilon\to0^+}\int_{-\frac{\Lambda\beta}{2a}+\mathrm{i}\varepsilon}^{\infty+\mathrm{i}\varepsilon}\mathrm{d}\omega\frac{\omega^2\tilde S - t}{\sqrt{W}}\frac{1}{\mathrm{e}^{a\omega-\nu}+1}.
\end{aligned} \tag{39}$$

A partial integration (picking up a boundary term) then enables us to express the thermal expectation value in terms of the functions F_0, F_1 introduced above,

$$\langle\bar\psi\psi\rangle_{\mathrm{th}} = \frac{S(x)}{\pi}\left(F_1 - \frac{\pi}{Ng^2}\right) + \frac{F_0}{\pi\beta} + \frac{m_0}{Ng^2}. \tag{40}$$

In the minimum of the grand canonical potential, F_0 and F_1 vanish. This reduces equation (40) to equation (10), thereby establishing exact self-consistency of the scalar condensate.

We now comment on the practical procedure to determine the phase diagram and thermodynamics of the massive GN model within this framework. First, we have to eliminate the bare parameters Ng^2, m_0 and the cut-off Λ in the standard way. Since all UV divergences are due to vacuum effects, there are no new difficulties as compared to the $T = 0$ case. All we need is the vacuum gap equation

$$\frac{1}{Ng^2} = \frac{1}{\pi}(1+m_0)\ln\Lambda = \frac{1}{\pi}(\ln\Lambda + \gamma). \tag{41}$$

The dynamical fermion mass in the vacuum (set equal to 1) and the confinement parameter γ are physical parameters which are kept fixed while one lets $Ng^2 \to 0$, $m_0 \to 0$ and $\Lambda \to \infty$. Irrelevant divergent terms $-\Lambda^2/8\pi$ and $-\mu\Lambda/2\pi$ from the energy and baryon density of the Dirac sea can simply be dropped. An expression for the renormalized grand canonical potential in which the limit $\Lambda \to \infty$ can safely be taken is

$$\pi\beta^2\Psi_{\mathrm{ren}} = \lim_{\Lambda\to\infty}\left[\frac{\Lambda^2\beta^2}{8} + \frac{a^2\langle\tilde{S}^2\rangle}{2}(\ln\Lambda + \gamma - 1) - a\beta\gamma\langle\tilde{S}\rangle\right.$$
$$\left. - a\,\mathrm{Re}\lim_{\varepsilon\to 0^+}\int_{-\frac{\Lambda\beta}{2a}+\mathrm{i}\varepsilon}^{\frac{\Lambda\beta}{2a}+\mathrm{i}\varepsilon}\mathrm{d}\omega\frac{\omega(\omega^2 - s + u)}{\sqrt{W}}\ln\left(2\cosh\frac{a\omega - \nu}{2}\right)\right]. \tag{42}$$

In principle, we have to solve the three equations $F_i = 0$ simultaneously. It is worthwhile to examine more closely the way in which F_i depend on the six relevant parameters $(a, b, \kappa, \gamma, \nu, \beta)$, since this suggests a simpler strategy of how to minimize Ψ. We first note that F_2 is a convergent integral which does not require any regularization or renormalization. Since F_2 depends neither on γ nor on β, the equation

$$F_2(a, b, \kappa, \nu) = 0 \tag{43}$$

can be solved for a, say, for given b, κ, ν. Now let us focus on the γ, β dependence of the other two equations. F_0 is also free of divergences. All we have to do here is to replace the ratio of bare parameters $\pi m_0/Ng^2$ by γ. The equation $F_0 = 0$ is then turned into

$$\gamma\beta = at\,I_0(a, b, \kappa, \nu), \tag{44}$$

where I_0 can be inferred from equation (37). The integral in F_1, on the other hand, has a logarithmic divergence at the lower integration limit. Isolating the divergence and eliminating $1/Ng^2$ with the help of the gap equation (41), the $\ln\Lambda$ terms are cancelled and the equation $F_1 = 0$ assumes the form

$$\gamma - \ln\beta = I_1(a, b, \kappa, \nu). \tag{45}$$

Equations (44) and (45) can be combined into

$$\gamma + \ln\gamma = I_1 + \ln(at\,I_0), \qquad \beta = at\,I_0/\gamma. \tag{46}$$

The first of these equations can be solved for γ, the second one then yields an explicit expression for β. In total, we have reduced the problem of finding the minimum of a function of three variables to the simpler problem of finding the zeros of two functions of one variable each.

Throughout this section, we have made use of complex integration so as to exhibit the formal structure of various expressions and the self-consistency in the most transparent way. In order to actually compute the one-dimensional numerical integrals in Ψ and in F_i, it is advisable to convert the integrals back to standard real integrals over the allowed energy bands. For more technical details and explicit expressions for I_0, I_1, F_2, we refer the reader to [30].

5. The full phase diagram of the Gross–Neveu model

In the previous section, we have outlined how to minimize the grand canonical potential given the three-parameter ansatz for $S(x)$. This can be used to evaluate bulk thermodynamic observables for any given T, μ and γ. In the present section, we turn to the structure of the phase diagram, including the location of the phase boundaries, the order of the transitions and the symmetries of the various phases. The following considerations have proven useful for this purpose. We expect phase transitions between a crystal phase and a homogeneous phase where $S(x) = M$ is constant. In the chiral limit, we can further distinguish between a chirally restored phase ($M = 0$) and a massive, chirally broken phase ($M > 0$). We therefore first need to understand for which choice of parameters $S(x)$, equations (15), (19), goes over into a constant. The elliptic modulus κ varies between 0 and 1. At the two boundaries of this interval, we find

$$\lim_{\kappa\to 0} \tilde{S} = \cot b, \qquad \lim_{\kappa\to 1} \tilde{S} = \coth b + \tanh \xi - \tanh(\xi + b). \tag{47}$$

The first limit is a constant, the second describes the single baryon profile. Clearly, both limits are relevant for phase boundaries where $\tilde{S}$ goes over from a periodic function in the crystal phase to a constant one in the massive Fermi gas phase ($M = A \cot b$ or $A \coth b$, respectively). As far as b is concerned, important special values are $b = 0$ and $b = \mathbf{K}$ with

$$\lim_{b\to 0} b\tilde{S} = 1, \qquad \lim_{b\to \mathbf{K}} \tilde{S} = \kappa^2 \frac{\mathrm{sn}\,\xi\,\mathrm{cn}\,\xi}{\mathrm{dn}\,\xi}. \tag{48}$$

The value $b = 0$ is the only value of b where $\kappa = 0$ and $\kappa = 1$ can coexist and therefore plays a prominent role in the phase diagram. In the chiral limit, b takes on the value $\mathbf{K}$. If we let $b \to \mathbf{K}$ and $\kappa \to 0$ simultaneously, $\tilde{S}$ vanishes and we can connect the crystal phase continuously to a chirally restored phase.

These observations are the key for computing the phase boundaries separating the crystal phase from the Fermi gas. Evidently, they are only applicable if the phase transitions are continuous, but this is indeed what we find. For $\kappa = 0$ or 1, the functions F_i further simplify, so that the actual computation along the lines described in section 4 is quite manageable. We have computed lines of constant b and constant ν, since this is most easily done in our scheme. For each value of κ, a certain (b, ν)-grid is mapped onto a two-dimensional surface in (γ, μ, T)-space by minimizing the grand potential. The resulting curved surface represents a second-order phase boundary.

We now turn to the numerical results, starting with the chiral limit $\gamma = 0$ and focusing on the phase boundaries. These are depicted in figure 4 which supersedes figure 1. The second-order line AB of the old phase diagram is unaffected. The first-order line BD of figure 1 is replaced by two second-order lines delimiting a novel kink–antikink crystal phase. The tricritical point B is turned into another kind of multicritical point labelled P_{L} in figure 4, located at precisely the same (μ, T) values. As we switch on γ (figure 5), the second-order line separating massive ($M > 0$) and massless ($M = 0$) phases disappears as a consequence of the explicit breaking of chiral symmetry. The crystal phase survives at all values of γ, but is confined to decreasing temperatures with increasing γ. For fixed γ, it is bounded by two second-order lines joining in a cusp. The cusp coincides with the critical point of the old phase diagram but has once again a significantly different character. The crystal phase exists and is thermodynamically stable inside the tent-like structure formed out of two sheets denoted as I and II. These sheets are defined by $\kappa = 0$ (I) and $\kappa = 1$ (II), respectively. The line $\mathrm{P_tC}$ where they join corresponds to $b = 0$ and coincides with line $\mathrm{P_tC}$ in figure 2. The baseline of sheet II in the (μ, γ)-plane has a simple physical interpretation: it reflects the γ-dependence

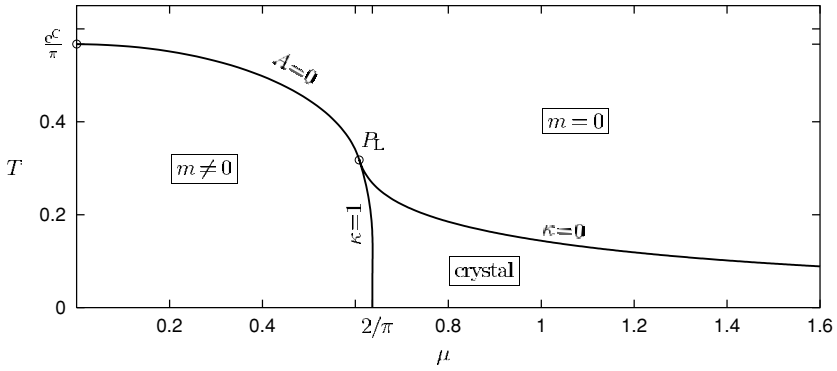

Figure 4. Phase diagram of the GN model in the chiral limit [28, 32]. All phase boundaries correspond to second-order transitions.

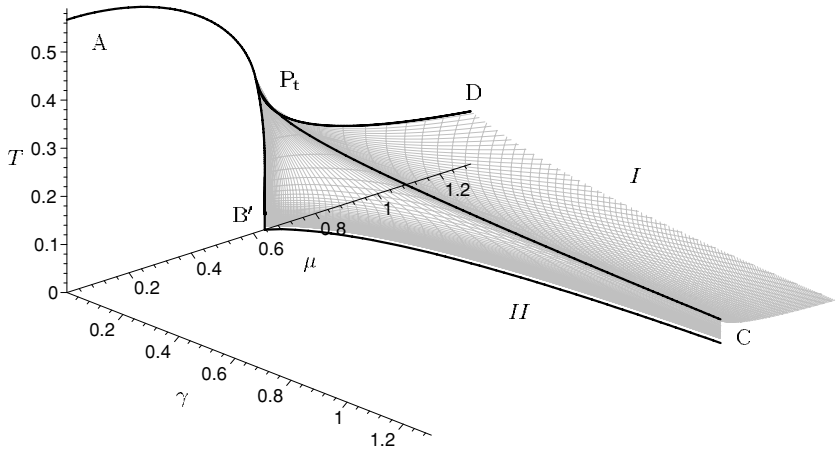

Figure 5. Revised phase diagram of the massive Gross–Neveu model [14, 30]. The shaded surfaces I, II separate the kink–antikink crystal from a massive Fermi gas and correspond to second-order phase transitions. The $\gamma = 0$ plane is the same as figure 4.

of the baryon mass in the massive GN model or, equivalently, the critical chemical potential at $T = 0$. The chiral limit $\gamma \to 0$ can be identified with $b \to \mathbf{K}$.

Another view of the phase diagram is displayed in figure 6. Here, we plot the phase boundaries in the (μ, T)-plane for several values of γ. These two-dimensional graphs correspond to cutting the three-dimensional graph in figure 5 by (equidistant) planes $\gamma =$ constant. They provide a better view of how the two critical lines are joined in a cusp and exhibit that the region in which the crystal is thermodynamically stable shrinks with increasing bare fermion mass.

The cusp line where the sheets I and II are glued together can be determined by taking the limit $b \to 0$ in F_i. As discussed above, in this limit the scalar potential becomes both homogeneous and κ-independent. One can show analytically that the resulting equations $F_i = 0$, for $i = 0, 1, 2$, are equivalent to the conditions $\Psi' = 0$, $\Psi'' = 0$, $\Psi''' = 0$ ($' = \partial_M$) for the translationally invariant calculation [12]. Hence, the curve $b = 0$ in the new phase diagram

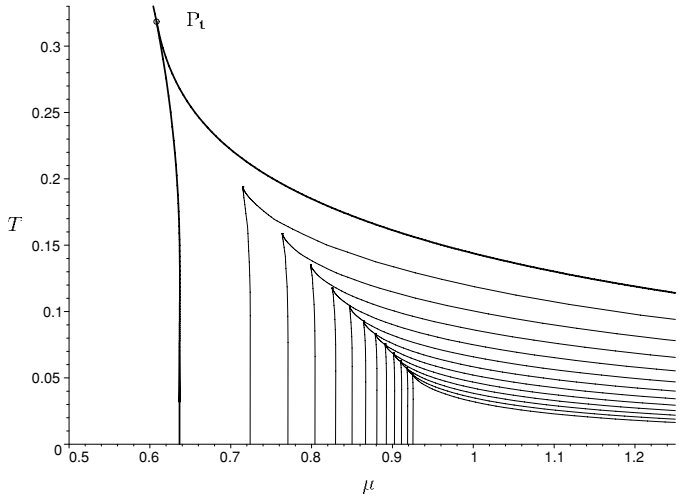

Figure 6. Two-dimensional sections $\gamma = \text{const}$ through the phase diagram of figure 5. The fat lines belong to $\gamma = 0$, the thin lines to $\gamma = 0.1, 0.2, \ldots, 1.2$, from top to bottom. The position of the cusp agrees with the critical point in the old phase diagram. From [30].

coincides with the line of critical points of the old phase diagram. One can also convince oneself that the critical first-order phase transition sheet shown in figure 2 is tangential to both sheets I and II along the line of endpoints.

6. Ginzburg–Landau theory near the tricritical point

In the vicinity of the tricritical point P_t, we can derive a Ginzburg–Landau effective action by expanding Ψ_{ren} in $a = \beta A$ [28, 30]. Since $S(x)$ is both weak and slowly varying there, this could also be obtained approximately without knowing the exact solution. Here, we turn things around and derive it via a Taylor expansion from the full expression. This should help to understand the character of the multicritical point.

We therefore start with an expansion of Ψ_{ren} in equation (42) in powers of a,

$$\pi\beta^2\Psi_{\text{ren}} = -\frac{\nu^2}{2} - \frac{\pi^2}{6} - \gamma\beta^2\langle S\rangle - \frac{\beta^2}{2}\langle S^2\rangle\left(\ln\frac{\beta}{4\pi} - \gamma\right) + a^2\sum_{n=0}^{\infty}\left(-\frac{a^2}{4\pi^2}\right)^n \frac{c_{n+1} + (u-s)c_n}{(2n+1)!}\,\mathrm{Re}\,\psi\left(2n, \frac{1}{2} + \frac{\mathrm{i}\mu}{2\pi T}\right). \tag{49}$$

Here, $\psi(n, z)$ is the polygamma function, the nth derivative of the digamma function $\psi(z) = \Gamma'(z)/\Gamma(z)$. The coefficients c_n can be obtained from a generating function,

$$\frac{\omega^3}{\sqrt{W}} = \sum_{n=0}^{\infty}\frac{c_n}{\omega^{2n}}. \tag{50}$$

One can now verify that the combinations $c_{n+1} + (u - s)c_n$ appearing in equation (49) are related as follows to spatial averages of powers of S and its derivatives with respect to x:

$$\begin{aligned} c_1 + (u-s)c_0 &= \frac{1}{2A^2}\langle S^2\rangle \\ c_2 + (u-s)c_1 &= \frac{3}{8A^4}(\langle S^4\rangle + \langle (S')^2\rangle) \\ c_3 + (u-s)c_2 &= \frac{5}{16A^6}\left(\langle S^6\rangle + \frac{1}{2}\langle (S'')^2\rangle + 5\langle S^2(S')^2\rangle\right). \end{aligned} \tag{51}$$

This enables us to write the Ginzburg–Landau effective action in the form

$$\Psi_{\text{eff}}(\gamma) = \Psi_{\text{eff}}(\gamma = 0) + \frac{\gamma}{2\pi}(S^2 - 2S), \tag{52}$$

where the effective action at $\gamma = 0$ is

$$\begin{aligned} \Psi_{\text{eff}}(\gamma = 0) = &-\frac{\pi}{6}T^2 - \frac{\mu^2}{2\pi} + \frac{1}{2\pi}S^2\left[\ln(4\pi T) + \operatorname{Re}\psi\left(\frac{1}{2} + \frac{\mathrm{i}\mu}{2\pi T}\right)\right] \\ &- \frac{1}{2^6\pi^3T^2}(S^4 + (S')^2)\operatorname{Re}\psi\left(2, \frac{1}{2} + \frac{\mathrm{i}\mu}{2\pi T}\right) \\ &+ \frac{1}{2^{11}3\pi^5T^4}\left(S^6 + \frac{1}{2}(S'')^2 + 5S^2(S')^2\right)\operatorname{Re}\psi\left(4, \frac{1}{2} + \frac{\mathrm{i}\mu}{2\pi T}\right). \end{aligned} \tag{53}$$

The instability with respect to crystallization is related to the fact that the 'kinetic' term $\sim(S')^2$ can change sign, depending on μ and T. We will come back to this formula in section 11 where we point out that it has a literal correspondence in condensed matter physics, namely in the theory of inhomogeneous superconductors.

Note that if one drops all derivatives of S in the effective action, one gets the result for the GN model under the assumption of unbroken translational invariance. The tricritical point for instance is defined by the simultaneous vanishing of the S^2 and S^4 coefficients which happens at $\mu_t = 0.608\,221$, $T_t = 0.318\,329$. Since the coefficients are the same as in the full effective action, we can understand why the tricritical point stays at the same place even though we allow for x-dependent potentials.

7. More about the chiral limit

In [28, 32], a number of additional results have been obtained in the chiral limit $\gamma = 0$. Here, we give a selection of figures and formulae to highlight certain features of this simpler special case.

We first reiterate that only at $\gamma = 0$ we are dealing with three distinct phases: the crystal, a massive and a massless Fermi gas. The scalar potential can be obtained by letting $b \to \mathbf{K}$ in equations (15), (19),

$$\tilde{S}(\xi) = \kappa^2\frac{\operatorname{sn}\xi\,\operatorname{cn}\xi}{\operatorname{dn}\xi} = \kappa^2\operatorname{sn}\xi\,\operatorname{sn}(\xi + \mathbf{K}) \tag{54}$$

and has a higher symmetry than for $\gamma \neq 0$, namely

$$S(x + \ell/2) = -S(x) \tag{55}$$

where ℓ is the spatial period. This is actually a remnant of the original discrete chiral symmetry of the model. Translational invariance and the γ^5 transformation both break down, leaving the unbroken discrete symmetry (55), i.e., a translation by half a period combined with a γ^5 transformation.

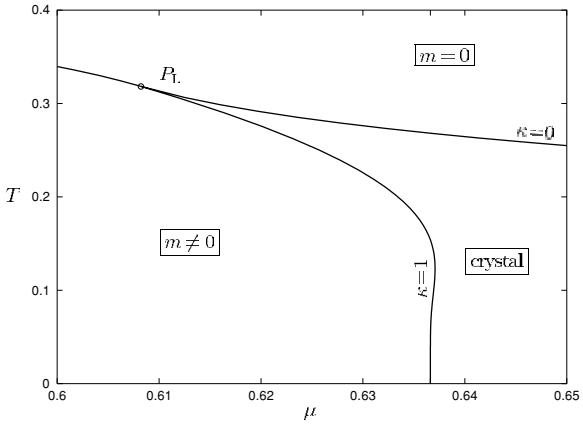

Figure 7. Close-up on the phase boundary between homogeneous and inhomogeneous ordered phases ($\kappa = 1$). Note the different scale on the μ-axis as compared to figure 4. From [28].

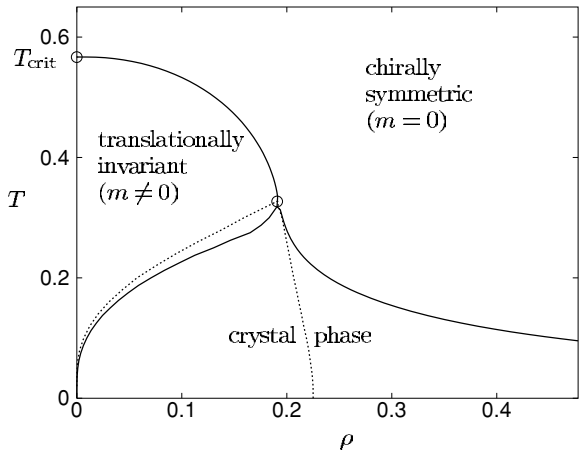

Figure 8. Revised phase diagram of the GN model in the (T, ρ)-plane [32]. The dashed lines belong to the old phase diagram, where they enclose the mixed phase. This 'droplet' region is superseded by the crystal phase featuring baryons.

An expanded plot which reveals more details about the shape of the phase boundary separating crystal and massive Fermi gas (labelled $\kappa = 1$) is displayed in figure 7.

A way of presenting the phase diagram complementary to that in figure 4 is given in figure 8 where we have transformed all phase boundaries from the (T, μ)- into the (T, ρ)-plane. Here, the first-order line of the old solution splits up into the two dashed lines which delimit the mixed phase region (droplets of chirally restored matter in the chirally broken vacuum). This should be replaced now by the two solid lines going downward from the tricritical point and enclosing the crystal phase. At $T = 0$, in particular, the crystal phase is stable at all densities.

As we approach the $\kappa = 0$ phase boundary, $S \sim \cos 2qx$ (with an amplitude vanishing at $\kappa = 0$), and the wave number q can serve as order parameter for the breakdown of translational invariance. In figure 9, we show the dependence of this order parameter on μ as

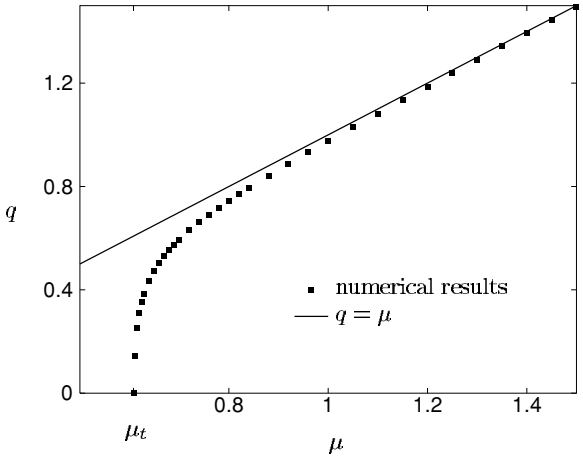

Figure 9. Wave number characterizing the crystal period along the phase boundary, showing a continuous phase transition at the tricritical point μ_t. From [32].

one moves along the phase boundary. The solid line is the curve $q = \mu$ which is approached asymptotically by the full calculation. At $\mu = \mu_t$, the tricritical point of the old solution, we see a clear signal of a second-order phase transition with breakdown of translational invariance.

Since the phase boundaries are of particular interest and easier to compute than other thermodynamic quantities, let us give the explicit formulae derived in [28] from which they can be obtained.

The boundary between the chirally restored phase and the crystal is characterized by $\kappa = 0$. It can either be derived by almost degenerate perturbation theory [32] or from the full thermodynamic potential. In the latter case, a straightforward expansion around $\kappa = 0$ yields

$$\ln \frac{1}{4\pi T} = \frac{1}{2} \min_{a \geqslant 0} \operatorname{Re} \left[\psi \left(\frac{1}{2} + \frac{\mathrm{i}}{2\pi}(\nu + a) \right) + (a \to -a) \right]. \tag{56}$$

The resulting curve is labelled '$\kappa = 0$' in figures 4 and 7. The asymptotic behaviour for large μ can also be determined,

$$T_{\mathrm{crit}} = \frac{\mathrm{e}^C}{4\pi\mu}. \tag{57}$$

The phase boundary does not reach the $T = 0$ axis so that chiral symmetry is not restored at $T = 0$ no matter how high the density is, at variance with the naive expectation for an asymptotically free theory.

For small ν where $\operatorname{Re}\left[\psi\left(2, \frac{1}{2} + \frac{\mathrm{i}\nu}{2\pi}\right)\right] < 0$, the unique minimum is at $a = 0$. In this range of ν, the phase boundary does not touch the crystal region in the (μ, T)-diagram. It corresponds to the transition between the massless and the massive homogeneous solutions described by

$$\ln \frac{1}{4\pi T} = \operatorname{Re} \psi \left(\frac{1}{2} + \frac{\mathrm{i}\nu}{2\pi} \right). \tag{58}$$

Upon using $\psi(1/2) = -C - \ln 4$ ($C \approx 0.5772$ is the Euler constant), we reproduce the well-known value of the critical temperature at $\mu = 0$,

$$T_c = \frac{\mathrm{e}^C}{\pi}. \tag{59}$$

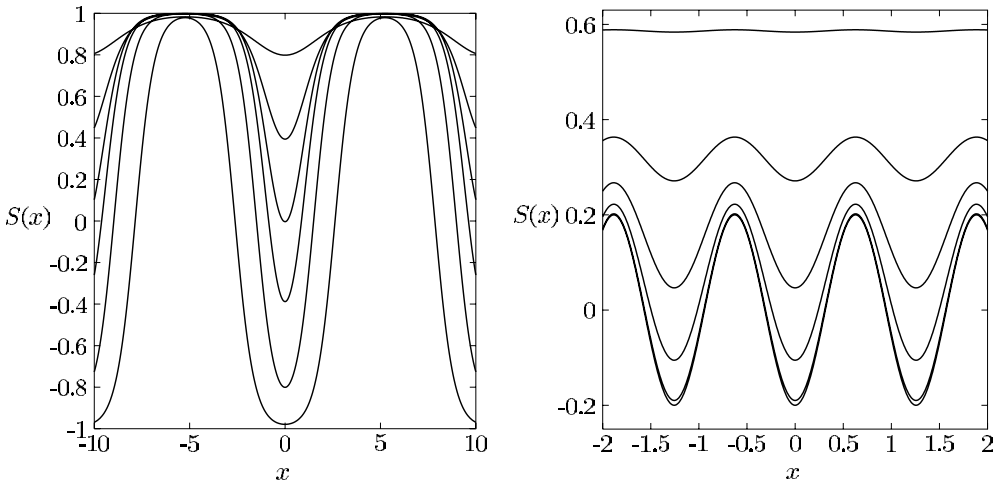

Figure 10. Self-consistent scalar potential $S(x)$ versus x for $p_f = 0.3$ (left) and $p_f = 2.5$ (right). From bottom to top: $\gamma = 0, 0.01, 0.1, 0.3, 0.75, 2.3$. From [31].

Next, we turn to the non-perturbative phase boundary at $\kappa \to 1$. It separates the crystal from the massive phase. The relation between a and ν along the phase boundary can be deduced from

$$\frac{\partial}{\partial a}\frac{1}{a}\int_0^{\pi/2} \mathrm{d}\varphi \frac{1}{\cos\varphi} \mathrm{Im}\ln\frac{\Gamma\left(\frac{1}{2}+\frac{\mathrm{i}}{2\pi}(\nu+a\cos\varphi)\right)}{\Gamma\left(\frac{1}{2}+\frac{\mathrm{i}}{2\pi}(\nu-a\cos\varphi)\right)} = 0. \tag{60}$$

With these values for a and ν,

$$-\ln\frac{\beta}{4\pi} + \frac{1}{\pi}\int_0^{\pi} \mathrm{d}\varphi\, \mathrm{Re}\,\psi\left(\frac{1}{2}+\frac{\mathrm{i}}{2\pi}(\nu+a\cos\varphi)\right) = 0 \tag{61}$$

yields β along the phase boundary. The resulting curve is shown in the phase diagram in figures 4 and 7 (label '$\kappa = 1$'). Equation (61) alone with values of (a, ν) that are not restricted by equation (60) gives the connection between a (or, equivalently, the effective fermion mass), ν and β in the massive phase outside the crystal region.

8. More about the zero temperature limit

Let us begin with some additional plots on cold, dense matter in the massive GN model [31]. First of all we wish to illustrate how the self-consistent scalar potential depends on γ. This is exhibited in figure 10 at low and high densities, respectively. The deepest curves always correspond to $\gamma = 0$, where the potential oscillates symmetrically around zero due to the residual symmetry (55). As we increase the symmetry violation parameter γ, the potential oscillates with decreasing amplitude around a value close to the mass M which the fermions would acquire in the translationally invariant solution. It is surprising that such a variety of potential shapes in the Dirac equation can all be reduced to the standard single gap Lamé equation.

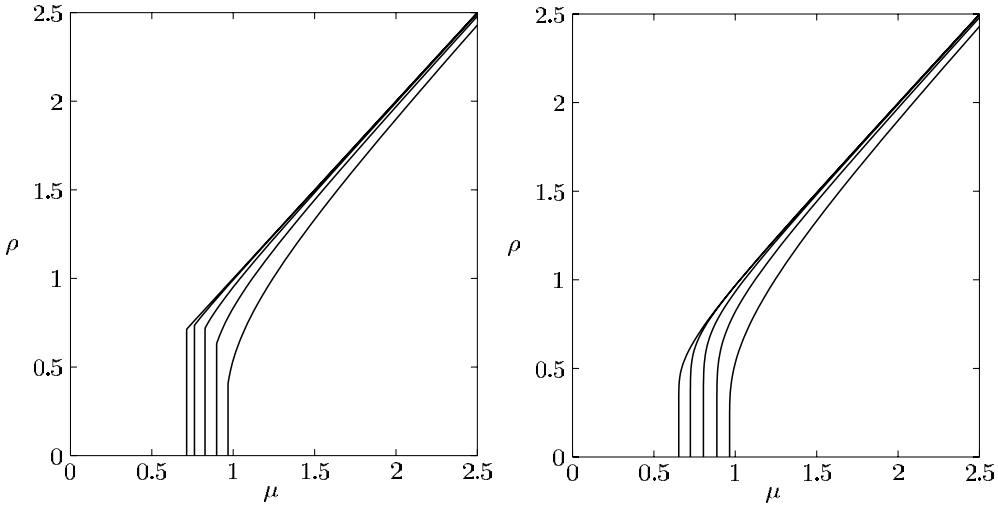

Figure 11. Baryon density versus chemical potential [31]. Left: (unstable) translationally invariant solution, showing a first-order transition. Right: (stable) crystal solution with second-order transition. Curves from left to right: $\gamma = 0.01, 0.1, 0.3, 0.75, 2.3$.

The next result which we should like to show is how the density varies with the chemical potential. At $T = 0$, the chemical potential can be obtained by differentiating the energy density with respect to the mean fermion density,

$$\mu = \frac{\partial E_{\text{g.s.}}}{\partial \rho}, \qquad \rho = \frac{p_f}{\pi}. \tag{62}$$

If we assume unbroken translational invariance (figure 11, left), we find discontinuities in these curves, confirming the result of [12] about a first-order phase transition. Repeating the same calculation for the crystal solution (which is the stable one), all the curves become continuous, signalling a second-order phase transition (figure 11, right). The critical chemical potential in this latter case coincides with the baryon mass, as expected on general grounds. By contrast, the first-order transition in figure 6 happens at a chemical potential which has at best the meaning of an approximate baryon mass in a kind of droplet model, cf the discussion in section 2.

The two real parameters which determine $S(x)$ at $T = 0$ are the elliptic modulus κ and the shift b. The scale factor A, on the other hand, is determined by the baryon density and κ,

$$A = \frac{2p_f \mathbf{K}}{\pi}. \tag{63}$$

Expression (63) implies that the mean density scales with the inverse spatial period of the potential, a consequence of the fact that the valence band is completely filled (for matter) or empty (for antimatter).

We now turn to additional analytic results. At $T = 0$, all integrals can be reduced to incomplete elliptic integrals of first, second and third types F, E, Π. We illustrate this fact in the case of the ground state energy and the self-consistency conditions. The ground state energy density is split up according to $E_{\text{g.s.}} = E_1 + E_2$ where E_1 is the sum over single particle energies of the occupied states, E_2 is the double-counting correction to the interaction energy.

For E_1, we get

$$\frac{2\pi}{A^2}E_1 = \left(2\frac{\mathbf{E}}{\mathbf{K}} - 2 + \kappa^2 - \frac{1}{2}\eta\right) + \left(2\frac{\mathbf{E}}{\mathbf{K}} - 2 - \eta\right)\ln\frac{\Lambda}{A\sqrt{2+\eta}} + \chi E(\tilde{p}, q) + \frac{\kappa^2}{\chi}\left(2\frac{\mathbf{E}}{\mathbf{K}} - 2 - \eta\right)[F(\tilde{p}, q) - \Pi(\tilde{p}, (\kappa')^2, q)] + \chi\left(2\frac{\mathbf{E}}{\mathbf{K}} - 2 + \kappa^2\right)F(\tilde{p}, q) \tag{64}$$

with the following definitions (η has been defined in equation (20)):

$$\chi = \sqrt{1+\eta}, \qquad \tilde{p} = \mathrm{dn}\, b, \qquad q = \kappa'/\mathrm{dn}\, b. \tag{65}$$

E_2, on the other hand, coincides with Ψ_2 in equation (25) since the HF double-counting correction is T-independent. After renormalization and upon using the vacuum gap equation together with equations (28), one finds

$$E_2 = \frac{A^2}{2\pi}(\gamma + \ln\Lambda)(s - 1 + 2u - \kappa^2) - \frac{A}{\pi}\gamma(\mathrm{Z} + t/s). \tag{66}$$

When adding up E_1 and E_2, the logarithmic divergence drops out and a finite result depending only on physical parameters is obtained.

Consider the self-consistency condition next. For $\gamma \neq 0$, it can be cast into the form

$$\begin{aligned} 0 &= A\,\mathrm{cn}\, b F(\tilde{p}, q) - \gamma\,\mathrm{sn}^2 b, \\ \gamma &= A\,\mathrm{cn}\, b[\kappa^2\Pi(\tilde{p}, (\kappa')^2, q) + \chi(\gamma + \ln(A\sqrt{2+\eta}))]. \end{aligned} \tag{67}$$

The original x-dependent condition has been transformed into two x-independent equations. They determine κ and b for given p_f and γ.

We finish this section with a few words about the high-density limit where the calculation becomes perturbative (see [31]). We use almost degenerate perturbation theory, following the standard weak coupling approach from solid state physics textbooks. In the double-counting correction, we have to take into account the bare fermion mass, and we allow for $S_0 \neq 0$ in addition to $S_{\pm 1} \neq 0$ (S_ℓ are the Fourier components of the periodic potential $S(x)$). Thus, our present ansatz for $S(x)$ is

$$S(x) = S_0 + 2S_1\cos(2p_f x). \tag{68}$$

The approximate energy density becomes

$$E_{\mathrm{g.s.}} = -\frac{\Lambda^2}{8\pi} + \frac{p_f^2}{2\pi} + \frac{S_0^2}{2\pi}\ln(2p_f) + \frac{\gamma}{2\pi}\left(S_0^2 - 2S_0\right) - \frac{S_1^2}{4\pi} + \frac{S_1^2}{4\pi}\ln(4p_f S_1) + \frac{\gamma}{\pi}S_1^2. \tag{69}$$

Minimizing with respect to S_0 and S_1, we find

$$S_0[\ln(2p_f) + \gamma] - \gamma = 0, \qquad S_1[2\gamma + \ln(4p_f S_1)] = 0. \tag{70}$$

The first equation has the unique solution

$$S_0 = \frac{\gamma}{\gamma + \ln(2p_f)}. \tag{71}$$

The second equation has two solutions: $S_1 = 0$, corresponding to unbroken translational invariance, and

$$S_1 = \frac{1}{4p_f}\,\mathrm{e}^{-2\gamma} \tag{72}$$

for the soliton crystal. Comparing the energy densities of these two solutions,

$$E_{\mathrm{g.s.}}(S_1 \neq 0) - E_{\mathrm{g.s.}}(S_1 = 0) = -\frac{1}{64\pi p_f^2}\,\mathrm{e}^{-4\gamma}, \tag{73}$$

we learn that the crystal is favoured, but the energy difference decreases rapidly with increasing γ. We have shown this simple calculation in detail since it proves non-restoration of translational invariance at high density for arbitrary bare fermion mass.

9. More about the double limit $T = 0$, $\gamma = 0$

The simplest problem beyond individual baryons and the first one which could be solved analytically [33] is the ground state of baryonic matter in the chiral limit. The ansatz for the reduced HF potential has the form (54), whereas the scale factor A is given by equation (63). Thus, only a single variational parameter κ is left. As expected, all analytical formulae of the previous section simplify tremendously in the chiral limit. Thus, for instance, the renormalized ground state energy density can now be expressed entirely in terms of complete elliptic integrals

$$E_{\text{g.s.}} = \frac{p_f^2 \mathbf{K}}{\pi^3}(4\mathbf{E} + (\kappa^2 - 2)\mathbf{K}) + \frac{2p_f^2 \mathbf{K}}{\pi^3}(2\mathbf{E} + (\kappa^2 - 2)\mathbf{K}) \ln\left(\frac{\pi}{2p_f \kappa \mathbf{K}}\right). \tag{74}$$

Minimizing with respect to κ yields the transcendental equation

$$\kappa = \frac{a}{\ell} = \frac{\pi}{2p_f \mathbf{K}}, \tag{75}$$

and self-consistency can be ascertained rather easily in this case. Eliminating p_f from $E_{\text{g.s.}}$ with the help of relation (75), we arrive at the following parametric representation of the ground state energy as a function of density in terms of the parameter κ:

$$E_{\text{g.s.}} = \frac{1}{4\pi} + \frac{1}{\pi\kappa^2}\left(\frac{\mathbf{E}}{\mathbf{K}} - \frac{1}{2}\right), \tag{76}$$

$$\frac{p_f}{\pi} = \frac{1}{2\kappa \mathbf{K}}. \tag{77}$$

In the low- or high-density limits, it becomes possible to systematically resolve the transcendental equation (77),

$$\begin{aligned} \kappa &\underset{p_f \to 0}{\approx} 1 - 8\,\mathrm{e}^{-\pi/p_f} + \frac{32(\pi + p_f)}{p_f}\,\mathrm{e}^{-2\pi/p_f}, \\ \kappa &\underset{p_f \to \infty}{\approx} \frac{1}{p_f} - \frac{1}{4p_f^3} + \frac{3}{64p_f^5}. \end{aligned} \tag{78}$$

For the energy as a function of density, one then finds

$$\begin{aligned} E_{\text{g.s.}} &\underset{p_f \to 0}{\approx} -\frac{1}{4\pi} + \frac{2p_f}{\pi^2} + \frac{8p_f}{\pi^2}\,\mathrm{e}^{-\pi/p_f}, \\ E_{\text{g.s.}} &\underset{p_f \to \infty}{\approx} \frac{p_f^2}{2\pi} - \frac{1}{2^6 \pi p_f^2} + \frac{3}{2^{14}\pi p_f^6}. \end{aligned} \tag{79}$$

In the low-density limit, the three terms correspond to the vacuum energy density, the contribution from the baryon mass ($\sim \rho M_B$ with $M_B = 2/\pi$) and a term reflecting the repulsive baryon–baryon interaction. At high densities, we can identify the free massless Fermi gas piece, the leading perturbative correction [32] and the next term coming from higher order effects, suggesting fast convergence.

We end this section with a few remarks about the baryon density. In the present case, the exact density is x-dependent and given by

$$\rho(x) = \frac{1}{2\kappa \mathbf{K}} - \frac{\mathbf{K}'}{2\pi\kappa}(\tilde{S}^2(x/\kappa) - \langle\tilde{S}^2\rangle). \tag{80}$$

It has the following high and low-density limits: at low density ($\kappa \to 1$), we recover the result for a single baryon

$$\rho(x, \kappa \to 1) \approx \frac{1}{4\cosh^2 x} + \frac{1}{4\cosh^2(x/\kappa + \mathbf{K})}. \tag{81}$$

At high density ($\kappa \to 0$), the total baryon density approaches a constant,

$$\rho(x, \kappa \to 0) \approx \frac{1}{2\kappa \mathbf{K}}, \tag{82}$$

unlike the scalar potential which keeps oscillating around 0 with wave number $2p_f$.

10. A note on baryons

Single baryons are contained in the low temperature, low-density limit of the general formalism, at least those with completely filled or empty valence state. They have also been studied as such, first in the chiral limit [8] and more recently in the massive GN model [19, 20]. One finds that the scalar potential has the same shape as the $m_0 = 0$ baryon with partial filling of the valence level,

$$S(x) = 1 + y(\tanh\xi_- - \tanh\xi_+) \tag{83}$$

with

$$\xi_\pm = yx \pm \tfrac{1}{2}\,\mathrm{artanh}\, y, \tag{84}$$

where $m = 1$ and $y \in [0, 1]$ is the only variational parameter. It depends on the occupation of the pair of valence levels and γ. Evaluating the ground state energy M_B and varying with respect to y,

$$\frac{\partial M_B}{\partial y} = 0, \tag{85}$$

one obtains

$$\frac{\nu}{2} = \frac{\theta}{\pi} + \frac{\gamma}{\pi}\tan\theta \tag{86}$$

where we have introduced the angle θ via $y = \sin\theta$ ($0 \leqslant \theta \leqslant \pi/2$). Here, ν is the number of valence particles minus the number of holes in the negative energy valence state. The baryon mass at the minimum becomes

$$\frac{M_B}{N} = \frac{2}{\pi}[\sin\theta + \gamma\,\mathrm{artanh}(\sin\theta)]. \tag{87}$$

The phase boundary in the $T = 0$ plane of figure 5 perfectly agrees with the function $M_B(\gamma)$ evaluated from equations (86), (87) for $\nu = 1$. This was not the case in the old phase diagram of figure 2, confirming once again that the revised results are now internally consistent.

11. Relation to condensed matter physics

From the point of view of relativistic QFT, the GN model is viewed as a soluble model for strong interaction physics, exhibiting phenomena such as asymptotic freedom, chiral symmetry breaking, dynamical mass generation, meson and baryon bound states. On the other hand, it can model quasi-one-dimensional condensed matter systems in the vicinity of a half-filled band. In this context, it has enjoyed success in explaining real experimental data, something unthinkable in particle physics due to its toy model character. The two most striking examples which we are aware of are conducting polymers on the one hand and (quasi-one-dimensional) inhomogeneous superconductors on the other hand. The basic physics is the same in both cases and closely related to the Peierls effect [34] of a one-dimensional electron–phonon system—dynamical formation of a gap at the Fermi surface resulting in a crystal structure. Details are different though, in particular the identification of the chemical potential is more subtle in the second case. Since the relationship between the GN model and condensed matter systems has played an important role for establishing the phase diagram of the GN model during the last few years, let us discuss it in somewhat more detail.

11.1. The GN model and polyacetylene

Conducting polymers have had a tremendous success story, culminating in the 2000 Nobel Prize in chemistry for physicist A J Heeger and the chemists A G MacDiarmid and H Shirakawa (for a review, see [35]). A prominent example is *trans*-polyacetylene (PA). This polymer $(CH)_x$ possesses two 'dimerized', degenerate ground states with alternating short and long bonds (figure 12, left). Owing to a number of simplifying assumptions, its continuum description is mathematically equivalent to the symmetric ($m_0 = 0$) GN model, as was realized shortly after the seminal work of Su, Schrieffer and Heeger on the discrete model [9, 36–38]. Dimerization plays the role of (discrete) chiral symmetry breaking in relativistic QFT. Solitons appear as kink-like defects where a transition between the two degenerate ground states happens, polarons are kink–antikink bound states. These excitations are important for understanding the electrical conductivity properties of doped PA (doping changes the number of electrons and is analogous to changing baryon number in the GN model). The solitons in particular have attracted considerable attention in the context of fermion number fractionization of which they are a prime example [39–41]. Solitons and polarons have originally been analysed theoretically in close analogy with kink and kink–antikink baryons already known on the field theory side [8]. A good account of both the physics and the early history can be found in [42], where also the limitations of the equivalence between the GN model and the theory of PA are critically examined. More recently, this theme has been taken up again by others [43]. Here, let us only mention a few facts which help to understand the curious equivalence of a non-relativistic electron–phonon system with a relativistic QFT. Particle/antiparticle degrees of freedom correspond to particles and holes, the half-filled band to the Dirac sea. The role of the UV cut-off is taken over by the band width W (incidentally of the order of 10 eV in PA). The two spin components (which exist only in the condensed matter case) are mapped onto two flavours (i.e., the $N = 2$ GN model). In the widely used semi-classical approach, there is no difference between the condensed matter treatment and the large N limit used above. The linear ('ultra-relativistic') dispersion relation for the massless fermions arises from a linearization at the Fermi surface, the Fermi velocity playing the role of the velocity of light. The lattice distortion (or phonon) field in the adiabatic approximation corresponds to the auxiliary scalar field σ in the GN model, the gap parameter $\Delta(x)$ to the scalar potential $S(x)$ and the electron–phonon coupling λ to the coupling constant Ng^2. In the relativistic

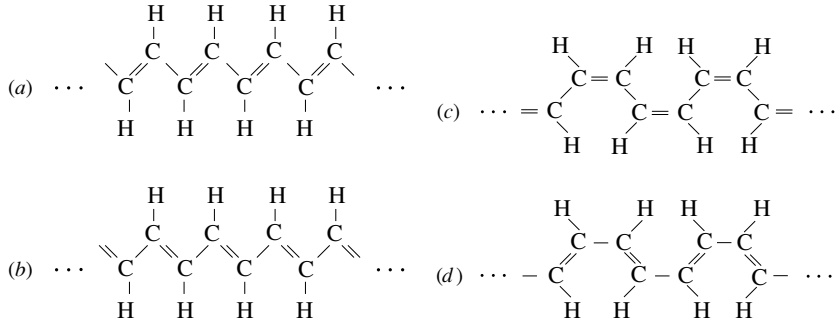

Figure 12. Left: two degenerate, dimerized ground states (*a*) and (*b*) of *trans*-PA, described theoretically in terms of the massless GN model. Right: two inequivalent configurations of *cis*-PA, leading to a description in terms of the massive GN model. Configuration (*c*) has lower energy than (*d*).

QFT case, one has to send the UV cut-off to infinity and the bare parameter Ng^2 to 0 in a specific way, dictated by the renormalizability of the model. In polymer physics, W and λ are physical observables to be taken from experiment. Nevertheless, in practice, these differences do not matter for many questions.

As mentioned above, the kink baryons are the solitons, the kink–antikink baryons the polarons, bipolarons and excitons of polymer physics. More specifically, for $N = 2$ the valence level can only be empty, fully occupied or half occupied. In condensed matter physics, there is then a relation between charge and spin. For the questions discussed in the present paper, fully occupied or empty valence levels are most relevant—these should be identified with the bipolarons. In the massless GN model, the baryon with fully occupied valence level becomes a kink/antikink at infinite separation; this is the reason why bipolarons are not discussed in the case of degenerate polymers like *trans*-PA.

If one starts to think about the massive GN model, it is not too hard to identify its condensed matter analogue: conducting polymers with non-degenerate ground states like *cis*-PA (figure 12, right). Their theoretical description was initiated by Brazovskii and Kirova [44] with the proposal that the gap parameter has two contributions, a constant, 'external' one arising from the basic structure of the polymer and an x-dependent, 'internal' one due to electron–phonon coupling,

$$\Delta(x) = \Delta_e + \Delta_i(x). \tag{88}$$

If we identify $\Delta(x)$ with the scalar mean field $S(x)$ and Δ_e with the bare mass m_0, we can immediately relate two problems from two different branches of physics. Baryons in the massive GN model then correspond to polarons and bipolarons in the polymer case [19, 42].

Now consider periodic solutions of the gap parameter for both degenerate and non-degenerate polymers and compare them with relativistic QFT. In the degenerate polymer case, polaron crystal solutions to the continuum model (at $T = 0$) have been found and discussed in [45–47]. They are mathematically identical to the ground state of baryonic matter in the chirally symmetric GN model, cf section 9. In some cases, the order parameter looks different from ours at first sight. However, the two expressions can be converted into each other by Landen's transformation for Jacobi functions in the form

$$\kappa \frac{\mathrm{sn}(\xi,\kappa)\mathrm{cn}(\xi,\kappa)}{\mathrm{dn}(\xi,\kappa)} = \frac{1-\kappa'}{\kappa}\mathrm{sn}\left((1+\kappa')\xi, \frac{1-\kappa'}{1+\kappa'}\right). \tag{89}$$

In the 1980s and 1990s, a lot of work was devoted to non-degenerate conducting polymers with the result that exact bipolaron lattice solutions were found by several groups. This suggests that the massive GN model should exhibit a soliton crystal at finite baryon density as well. It encouraged us to look for such solutions of the massive GN model and to try the functional form of the self-consistent scalar potential for non-degenerate polymers in the GN model. It has been derived by various methods such as inverse spectral theory [48], Poisson summation of periodic sums of single polarons [49–51] or relation to the Toda lattice [23]—a rich source of inspiration also for those working on relativistic QFT. Reference [24] contains a particularly thorough discussion and corrects misprints in some of the original papers. In section 3, we have in fact presented the functional form determined in these works and used it as ansatz in a relativistic HF calculation. The arguments given in favour of this ansatz are also borrowed from the condensed matter literature. On the other hand, we did not find the full phase diagram at finite T presented in section 5 in the polymer literature.

11.2. The GN model and inhomogeneous superconductors

Superconductivity is driven by fermion–fermion pairing (Cooper pairs), whereas the GN model features fermion–antifermion pairing (chiral symmetry breaking). We first have to understand how these two distinct physical phenomena are related to each other. Along the lines described in [52], one can actually map the GN Lagrangian onto a 'dual' Lagrangian which has fermion–fermion pairing by means of a canonical transformation. In the relativistic case, this is possible due to a two-dimensional remnant of the Pauli–Gürsey symmetry of massless fermions [53, 54] and explains why two seemingly different large N field theory models give identical results [55]. All one has to do is redefine particles into antiparticles for left-handed fermions only. If one works at non-zero chemical potential, a baryonic chemical potential μ in the GN model corresponds to an 'axial' chemical potential μ_5 in the dual BCS-type model. The phase diagram which we have discussed in section 5 (for $m_0 = 0$) is equivalent to the phase diagram of a theory with Lagrangian

$$\mathcal{L} = \sum_{n=1}^{N} \bar{\psi}^{(n)} \mathrm{i}\partial\!\!\!/ \psi^{(n)} + \frac{g^2}{2}\left[\sum_{n=1}^{N}\left(\psi_R^{(n)\dagger}\psi_L^{(n)\dagger} + \psi_L^{(n)}\psi_R^{(n)}\right)\right]^2, \tag{90}$$

provided we reinterpret the chemical potential $\mu = \mu_R + \mu_L$ as axial chemical potential $\mu_5 = \mu_R - \mu_L$. The kink–antikink phase of the GN model can then be identified with the Larkin–Ovchinnikov–Fulde–Ferrel (LOFF) phase [56, 57] of the dual model. Such inhomogeneous superconductors have recently attracted considerable attention in the context of QCD (for a review article, see [58]).

Let us now turn to non-relativistic condensed matter physics and demonstrate that the GN model can also be related to quasi-one-dimensional superconductors in nature. In 1981, Mertsching and Fischbeck addressed the quasi-one-dimensional Peierls–Fröhlich model with a nearly half-filled band, an electron–phonon system [59]. This is the same basic model as the continuum model for degenerate polymers [9], but here the phase diagram at finite temperature was considered, notably the transition between commensurate–incommensurate charge density waves. Comparing with our results at $m_0 = 0$, we find a mathematical one-to-one correspondence between this system and the GN model now extended to finite temperature. The authors of [59] have also found the analytic solution to the mean-field equation, guided by the Landau expansion around the triple point (which is called Leung point [60] in this context).

In a subsequent paper, Machida and Nakanishi [61] used the phase diagram of [59] in a different physics context: they studied the interplay of superconductivity and ferromagnetism in $ErRh_4B_4$ (erbium–rhodium–boride). They managed to reduce this problem mathematically

to the Peierls–Fröhlich model. For real order parameter, their results are again fully equivalent to ours for the GN model, except that now one has to use another dictionary: the Dirac equation corresponds to the Bogoliubov–deGennes (BdG) equation, flavour ($N = 2$) to spin (which exists in a quasi-one-dimensional world), chemical potential to magnetic field, baryon density to spin polarization. Our three phases (massive, crystal and massless) correspond to their BCS, 'sn' and normal phases, respectively. Not only the phase boundaries, but all observables can be identified if one keeps in mind the above-mentioned dictionary. Let us try to understand in more detail the reasons behind this remarkable correspondence. The BdG Hamiltonian involves four fermion fields, namely right (ψ_s) and left (ϕ_s) moving electrons with spin up ($s = +$) and spin down ($s = -$). This Hamiltonian can be mapped onto the Peierls–Fröhlich Hamiltonian by the canonical transformation

$$\begin{pmatrix} \psi_+ \\ \psi_- \\ \phi_+ \\ \phi_- \end{pmatrix} \longrightarrow \begin{pmatrix} \psi_+ \\ \psi_-^\dagger \\ \phi_- \\ \phi_+^\dagger \end{pmatrix}, \tag{91}$$

i.e., particle hole conjugation for spin-down fields followed by a spin-flip of left-moving fields. Under this transformation, spin density goes over into ordinary fermion density, and one can understand all other relationships as well.

Finally, we would like to mention the more recent work of Buzdin and Kachkachi [62]. They derive the Ginzburg–Landau theory for nonuniform LOFF superconductors near the tricritical point in the (T, H)-phase diagram in one, two and three dimensions. If we take their result for one dimension and specialize it to a real order parameter, we find perfect agreement between our equation (53) and their equation (3) in appropriate units. Once again we have to identify their magnetic field $\mathcal{H}_0$ with our chemical potential μ for the reasons discussed above.

12. Concluding remarks

At the time of writing our previous review article on the thermodynamics of two-dimensional quantum field theories [5], some progress had been made on fermionic models with continuous chiral symmetry like the 't Hooft or the NJL_2 model. The fact that the existence of baryons implied a crystal structure of baryonic matter had been understood and the physical interpretation in terms of a gap at the Fermi surface—the 'rediscovery of the Peierls effect in relativistic QFT'—had been clearly stated. Towards the end of this paper, we identified areas where future work was needed, mentioning in particular the GN model with discrete chiral symmetry. We hope to have shown in the present work that this problem has been solved in the meantime, including the generalization to the massive model with explicit symmetry breaking. As a result, the situation is now reversed: today we know a lot more about the thermodynamics of the discrete chiral GN model than about the NJL_2 model, particularly in the presence of a bare mass term. For a long time, the phase diagram of the NJL_2 model was thought to be identical to that of the GN model, but this can now be ruled out due to their different baryon structure. It will be interesting to see whether one can make further progress on the phase diagram of the massive NJL_2 model where topology is expected to play a crucial role, analogous to the Skyrme model and Skyrme crystal in $3 + 1$ dimensions.

In [5], we also pointed out that this type of soluble QFT models still had the potential to surprise us after so many years of studies. If anything, this impression has only been reinforced since then. The simple Lagrangian (1) has generated a much richer phase diagram than previously thought, together with some beautiful mathematics. Even more surprising for us was perhaps the discovery that a relativistic QFT 'toy model' has such a close relationship

to various quasi-one-dimensional condensed matter systems. We have tried to cover these less familiar aspects of the GN model in the present work as well. They represent a good example for a fruitful exchange between condensed matter and particle physics. Originally, condensed matter physics, in particular polymer physics, could profit of the particle physicists know-how on soliton-like baryons in the GN model to understand for instance electrical conductivity properties. Subsequently, the polymer continuum models were vigorously developed, notably in the direction of crystal solutions where the expertise has traditionally been residing in condensed matter physics. During our work, we were able to take advantage of the progress in polymer physics to settle some unresolved issues in QFT, while at the same time generalizing the bipolaron lattice to finite temperature.

This whole process was not as straightforward as it may sound. It was not that easy for us to find the relevant information in the unfamiliar literature where it was often hidden under a lot of material of less interest to us. Thus, we could not avoid doing many things 'the hard way'. For example, the calculation of the phase diagram in the chiral limit, first numerically and then analytically, was performed by us independently of already existing pertinent results in the 'parallel world' of condensed matter physics. In any case, our study of the massive model has profited immensely from this interplay, and it was better to realize and exploit the relationship between these two different branches of physics late than never.

Acknowledgments

The author wishes to thank the guest editors of this special issue of J. Phys. A: Math. Gen., in particular Gerald Dunne, for the invitation to write this contribution. A most pleasant and productive collaboration with Oliver Schnetz and Konrad Urlichs on the work reported here is gratefully acknowledged. I also thank both of my collaborators for a critical reading of the manuscript.

References

[1] Gross D J and Neveu A 1974 *Phys. Rev.* D **10** 3235
[2] Mermin N D and Wagner H 1966 *Phys. Rev. Lett.* **17** 1133
[3] Coleman S 1973 *Commun. Math. Phys.* **31** 259
[4] Witten E 1978 *Nucl. Phys.* B **145** 110
[5] Schön V and Thies M 2001 *At the Frontier of Particle Physics: Handbook of QCD, Boris Ioffe Festschrift* vol 3, ed M Shifman (Singapore: World Scientific) chapter 33 p 1945
[6] Klein A 1976 *Phys. Rev.* D **14** 558
[7] Pausch R, Thies M and Dolman V L 1991 *Z. Phys.* A **338** 441
[8] Dashen R F, Hasslacher B and Neveu A 1975 *Phys. Rev.* D **12** 2443
[9] Takayama H, Lin-Liu Y R and Maki K 1980 *Phys. Rev.* B **21** 2388
[10] Nardulli G 2002 *Riv. Nuovo Cimento* **25N3** 1
[11] Wolff U 1985 *Phys. Lett.* B **157** 303
[12] Barducci A, Casalbuoni R, Modugno M, Pettini G and Gatto R 1995 *Phys. Rev.* D **51** 3042
[13] Klimenko K G 1988 *Theor. Math. Phys.* **75** 487
[14] Schnetz O, Thies M and Urlichs K 2005 The phase diagram of the massive Gross–Neveu model, revisited (*Preprint* hep-th/0507120)
[15] Treml T F 1989 *Phys. Rev.* D **39** 679
[16] Inagaki T, Kouno T and Muta T 1995 *Int. J. Mod. Phys.* A **10** 2241
[17] Schön V and Thies M 2000 *Phys. Rev.* D **62** 096002
[18] Karsch F, Kogut J and Wyld H W 1987 *Nucl. Phys.* B **280** 289
[19] Thies M and Urlichs K 2005 *Phys. Rev.* D **71** 105008
[20] Feinberg J and Hillel S 2005 *Phys. Rev.* D **72** 105009
[21] Pöschl G and Teller E 1933 *Z. Phys.* **83** 143

[22] Feinberg J 2004 *Ann. Phys., NY* **309** 166
[23] Saxena A and Bishop A R 1991 *Phys. Rev.* A **44** R2251
[24] Davids P S, Saxena A and Smith D L 1996 *Phys. Rev.* B **53** 4823
[25] Sutherland B 1973 *Phys. Rev.* A **8** 2514
[26] Dubrovin B A and Novikov S P 1975 *Sov. Phys. JETP* **40** 1058
[27] Whittaker E T and Watson G N 1980 *A Course of Modern Analysis* (Cambridge: Cambridge University Press)
[28] Schnetz O, Thies M and Urlichs K 2004 *Ann. Phys., NY* **314** 425
[29] Li H, Kusnezov D and Iachello F 2000 *J. Phys. A: Math. Gen.* **33** 6413
[30] Schnetz O, Thies M and Urlichs K 2005 Full phase diagram of the massive Gross–Neveu model (*Preprint* hep-th/0511206)
[31] Thies M and Urlichs K 2005 *Phys. Rev.* D **72** 105008
[32] Thies M and Urlichs K 2003 *Phys. Rev.* D **67** 125015
[33] Thies M 2003 *Phys. Rev.* D **68** 047703
[34] Peierls R E 1955 *Quantum Theory of Solids* (Oxford: Clarendon) p 108
[35] Heeger A J, Kivelson S, Schrieffer J R and Su W P 1988 *Rev. Mod. Phys.* **60** 781
[36] Su W P, Schrieffer J R and Heeger A J 1979 *Phys. Rev. Lett.* **42** 1698
[37] Campbell D K and Bishop A R 1981 *Phys. Rev.* B **24** 4859
[38] Campbell D K and Bishop A R 1982 *Nucl. Phys.* B **200** 297
[39] Jackiw R and Rebbi C 1976 *Phys. Rev.* D **13** 3398
[40] Jackiw R and Schrieffer J R 1981 *Nucl. Phys.* B **190** 253
[41] Niemi A J and Semenoff G W 1986 *Phys. Rep.* **135** 99
[42] Campbell D K 2002 *Synth. Metals* **125** 117
[43] Chodos A and Minakata H 1994 *Phys. Lett.* A **191** 39
[44] Brazovskii S A and Kirova N N 1981 *JETP Lett.* **33** 4
[45] Brazovskii S A, Gordyunin S A and Kirova N N 1980 *JETP Lett.* **31** 456
[46] Horovitz B 1981 *Phys. Rev. Lett.* **46** 742
[47] Horovitz B 1987 *Phys. Rev.* B **35** 734
[48] Brazovskii S A, Kirova N N and Matveenko S I 1984 *Sov. Phys.—JETP* **59** 434
[49] Saxena A and Gunton J D 1987 *Phys. Rev.* B **35** 3914
[50] Saxena A and Cao W 1988 *Phys. Rev.* B **38** 7664
[51] Saxena A and Gunton J D 1988 *Phys. Rev.* B **38** 8459
[52] Thies M 2004 *Phys. Rev.* D **69** 067703
[53] Pauli W 1957 *Nuovo Cimento* **6** 205
[54] Gürsey F 1958 *Nuovo Cimento* **7** 411
[55] Chodos A, Minakata H and Cooper F 1999 *Phys. Lett.* B **449** 260
[56] Fulde P and Ferrell R A 1964 *Phys. Rev.* **135** 550
[57] Larkin A I and Ovchinnikov Yu N 1965 *Sov. Phys.—JETP* **20** 762
[58] Casalbuoni R and Nardulli G 2004 *Rev. Mod. Phys.* **76** 263
[59] Mertsching J and Fischbeck H J 1981 *Phys. Status Solidi* b **103** 783
[60] Leung M C 1975 *Phys. Rev.* B **11** 4272
[61] Machida K and Nakanishi H 1984 *Phys. Rev.* B **30** 122
[62] Buzdin A I and Kachkachi H 1997 *Phys. Lett.* A **225** 341